H I velocity dispersion in NGC 1058

A. O. Petric

Astronomy Department, Columbia University, New York, NY USA
andreea@astro.columbia.edu

M. P. Rupen

National Radio Astronomy Observatory, P.O. Box O, Socorro, NM, 87801, USA
mrupen@aoc.nrao.edu

ABSTRACT

We present excellent resolution and high sensitivity Very Large Array (VLA) observations of the 21cm H I line emission from the face-on galaxy NGC 1058, providing the first reliable study of the H I profile shapes throughout the entire disk of an external galaxy. Our observations show an intriguing picture of the interstellar medium; throughout this galaxy velocity– dispersions range between 4 to 15 km s^{-1} but are not correlated with star formation, stars or the gaseous spiral arms. The velocity dispersions decrease with radius, but this global trend has a large scatter as there are several isolated, resolved regions of high dispersion. The decline of star light with radius is much steeper than that of the velocity dispersions or that of the energy in the gas motions.

Subject headings: galaxies: kinematics and dynamics — individual:NGC 1058; galaxies:ISM

1. Introduction

Observations of H I velocities perpendicular to the disk (v_z) are necessary for studies of both the interstellar medium (ISM) (McKee & Ostriker 1977, Kulkarni & Heiles 1988, Braun 1992, 1997) and disk dynamics (Oort 1932; Rupen 1987; Lockman & Gehman 1991; Merriefield 1993; Malhotra 1994, 1995; Olling 1995) because they set a direct upper limit on the thermal and kinetic temperature of the gas. Hence the H I velocities perpendicular to the disk are an important dynamical tracer and as such can be used to constrain, both the gas mass distribution in the plane and its vertical structure (i.e., density as a function of height-z above the plane)(van der Kruit & Shostak 1982,1984, Lockman & Gehman 1991, Malhotra 1995).

The behavior of the velocity dispersions as a function of galactic radius is important for determinations of the shape of dark matter halos. To date even the most sophisticated methods (e.g. Olling 1995, 1996) assume either a constant or an azimuthally symmetric velocity dispersion. Our measurements can therefore be used with studies of edge-on systems to determine radial variations in the mass to light (M/L) ratio.

Processes associated with star formation,such as stellar winds and multiple supernova explosions are thought to put energy into the ISM in the form of mechanical energy, starlight (which leads to photoelectric emission from dust grains), and cosmic rays. The velocity dispersion in the z direction is intimately connected to the forces holding the gas against gravitational instabilities and hence to star-formation in the disk (e.g. Mac Low & Klessen 2004, Li, Mac Low & Klessen 2005). Measuring the degree of correlation between the locations of star-forming regions and those of high dispersion is a good method to investigate the relation between star-related energy sources and H I bulk motions.

The face-on spiral galaxy NGC 1058 (e.g. Eskridge et al. 2002) is ideal for studies of H I v_z dispersions. Its low inclination (4°–11°) (Lewis 1987, van der Kruit & Shostak 1984) means that the gradient in rotational velocity is small across the beam and therefore it does not significantly corrupt measurements of velocities perpendicular to the disk.

Single dish studies of NGC 1058 (Allen & Shostak 1979, Lewis 1975, Lewis 1984) lack the resolution to trace the dispersion across the disk but through modeling of the rotational component these authors estimate it to range between 7 and 9 km/sec. In a series of papers (1982-1984) van der Kruit & Shostak analyze H I emission profiles in a number of face-on galaxies and determine that the velocity dispersions in NGC 1058 range only between 7 to 8 km/sec at all radii with very little variation. Dickey, Hanson, & Helou (1990) find the that velocity dispersion in NGC 1058 decreases with optical surface brightness but that in the extended gas disk, beyond the Holmberg radius the velocity dispersion is 5.7 km/sec everywhere, that is no variations with spiral phase or H I surface density are found.

All previous determinations of the H I velocity dispersion in NGC 1058 have been hindered by low spatial (e.g., Lewis 1984) and/or spectral (e.g., van der Kruit & Shostak 1984) resolution as well as by relatively poor sensitivity, requiring smoothing over large sections of the galactic disk, or missing up to 40% of the total flux (Dickey, Hanson, & Helou 1990). These trade-offs have led to significantly different conclusions about the H I velocity dispersion. Our sensitive observations at high spatial and velocity resolution as well as recovery of the entire single dish flux, allowed us to accurately measure the profile widths even in the outskirts of the H I disk, to resolve the arm from the interarm regions, and to analyze in detail the H I profile shapes, not just their breadths throughout the H I disk.

2. Observations and Data Reductions

The 21cm line of neutral hydrogen in NGC 1058 was observed with the VLA in the C and CS[1] configurations. The C configuration data was taken on 14 and 15 June 1993 for a total time on-source of 12.23 hours. The D configuration observation were performed on 7 and 8 November 1993 for a total time on source of 2.67 hours, and CS configuration data was collected on January 3, 1995 for a total time on-source of 5.42 hours. Rupen (1997,1998) gives a detailed account of the UV coverage in each of the configurations, compares the merits of each configuration, and discusses the benefits of combining them.

Both the C and CS configurations have a maximum baseline of 3.6 km, while the D configuration has a maximum baseline 1 km). The minimum baseline, which determines the size of the most extended feature which can be observed by the VLA, is 35 m. All observations were taken in dual polarization mode and Hanning smoothing was applied on-line; resulting in 127 independent spectral channels with a velocity width of 2.58 km/sec. We followed the normal AIPS calibration procedures and used the same flux (3C48) and phase (0234+285) calibrators throughout. The continuum emission was approximated as a linear fit to visibilities in 20 line-free channels on each side of the signal, and this fit was then subtracted from the *uv*-data in all the channels. Rupen (1999), gives a detailed description of the bandpass calibration and continuum subtraction.

The data cube presented here was deconvolved using the CLEAN algorithm as implemented by AIPS task IMAGR.[2], iterated until the residuals were nearly zero and the flux density in the CLEAN model was stable. The cube was tapered to a resolution of $30'' \times 29''$, or 1.3×1.3 kpc at a distance of 10 Mpc (Ferguson et al. 1998). Rupen (1997), presents a detailed comparison of several cleaning algorithms and motivates the use of the CLEAN algorithm for this data. A more general discussion of CLEAN as implemented in AIPS is given in chapter 5, of the AIPS cookbook as well as in Cornwell, Braun, & Briggs 1999. A more specific examination of deconvolution algorithms as applied on our NGC 1058 data is presented in Rupen (1997,1999).

The RMS noise level in the line channels of the cube was 0.5 and mJy/beam, corresponding to a column density of 1.6×10^{18} cm^{-2} per channel. The H I integrated line profile

---

[1] The CS (shortened C) configuration moves two antennas from intermediate stations in the standard C configuration to the center of the array. The resulting short spacings significantly increase the sensitivity of the array to extended structure, while maintaining the same spatial resolution (Rupen 1997).

[2] A description of IMAGR can be found in the AIPS cookbook available online at http://www.aoc.nrao.edu/aips/cook.html.

agrees with those obtained in single dish studies (Allen & Shostak 1979) after both the single dish and the VLA data are corrected for primary beam response.

Figure 1 presents the frames of the $30''$ data cube. Each image (traditionally called a channel map) in this figure represents the 21 cm line emission at a certain velocity, the abscisa and ordinate axis are the RA and Dec coordinates. The lack of artifacts in these images (such as a negative bowl around the galaxy) also suggests that the images have been correctly deconvolved.

3. Results and Analysis

The general properties of NGC 1058 are presented in Table 1. Figure 2 shows intensity weighted mean velocity contours atop the H I intensity map and presents the H I spiral structure of NGC 1058. Figure 2 also illustrates the superb sensitivity and resolution of these studies, which allowed us to measure the H I emission at distances of approximatively 10 kpc from the center of the disk and to differentiate between the arms and the inter-arms. We characterize the widths of the H I profiles by the relative dispersions $\sigma_{\rm v}$ of the best Gaussian fit [3]; the fits were done using a least squares minimization algorithm.

Figures 3 and 4, show the observed profiles for a few pixels throughout NGC 1058 from the $45''$ and the $30''$ data sets respectively. The single Gaussians which best approximate the shapes of these profiles, as well as their residuals are also shown. Note, that each of the profiles is representative of the remainder of the spectra, it is not a *best find* or the result of averaging over large areas of the disk or velocity space.

While the residual patterns suggest that a single Gaussian is not a good functional description of the H I profiles in NGC 1058, the FWHM and σ_v derived from the single Gaussian fits track well the intrinsic width of the H I spectrum. This proportionality allows us to describe the widths of the profile in terms of the results of our least squares fitting. The general characteristics of the velocity dispersion will be discussed in terms of the $45''$ and $30''$ cubes.

---

[3] The FWHM is often use to characterize the H I line widths. This *tradition* is based upon the fact that H I profiles are modeled by one or multiple Gaussians, where the flux as a function of velocity v is given by

$$f(v) = \frac{1}{\sigma\sqrt{2\pi}} exp\left[-\left(\frac{1}{2\sigma_{\rm v}{}^2}\right)(v - v_0)^2\right]$$

and v_0 is the velocity at associated with the peak flux.

4. General Characteristics of the Velocity Dispersion

Figure 5 presents the distribution of velocity dispersions across the disk of NGC 1058. Unlike previous observers of NGC 1058, we find a wide range of dispersions from 4 to 14 km sec^{-1} in addition to a few extremely narrow profiles with $\sigma_v \sim 3.5$ km sec^{-1}. These narraow profiles are found in regions of relatively low column density at radii greater than 300$''$ or 13 kpc. There are three regions of high dispersion which stand out in Figure 5: one in the center (labeled C and ~ 4.5 kpc across) and two others symmetric about the center in the North-West (N ~ 3 kpc) and South-East (S $\sim$ 3×5 kpc) of the center. We find no obvious correlation between high H I velocity dispersion and stars or star formation tracers such as H_α (Figure 10), radio contiuum, SNe except in the central region C. The most probable explanation for the observed highest dispersions outside the central region (i.e. in N and S) are small scale (≤ 0.7 kpc) bulk motions (see section 7 below). In the southern, part the disk could be warping (van der Kruit & Shostak 1984, Shen & Sellwood 2006) leading to the observed broad profiles. Figure 6 shows that H I profiles from N and S are also assymmetric. However, a similar explanation for region N would suggest rather impressive small-scale structure in the warp as it would requiere the inclination to change ~ 3 degrees over a region smaller than 0.7 kpc in diameter, if we assume from Tully Fisher an intrinsic rotation velocity of 150 km s^{-1} . A more exciting alternative explanation for the bulk motions observed in N is that they are caused by the infall of gas left over from galaxy formation. However, this is somewhat difficult to reconcile with the relatively low column density in these regions.

Two global trends are evident from the derived dispersions: a radial fall-off, shown in Figure 7, and a predominance of the broadest profiles in the inter-arm regions of the galaxy (Figure 9). Ferguson et al. (1998) used deep $H\alpha$ observations to reveal the presence of H II regions in the central 6 kpc of NGC 1058. There are several knots of high dispersion (12 to 13.5 km/sec) in region C, with most of the profiles measuring between 7.5 and 11 km/sec. However, none of the star formation sites outside the central $\sim$2 kpc discovered in that study seem to affect the width of the profiles. Also, regions N and S are located in the inter-arm regions and are not associated with sufficiently strong star formation to be detected in the Ferguson et al. (1998) study. Therefore we find that the dispersions do not correlate with star formation as shown from the overlay of Feruson et al (1998)'s Hα map atop contours of velocity dispersion Figure 10.

Figure 8 shows the kinetic energy in the gas associated with motions perpendicular to the disk. Because only a qualitative behaviour was of interest here, the kinetic energy in vertical motions at a certain pixel location was roughly approximated as the product of total intensity times the square of the velocity dispersion. Approximated as such, the kinetic

energy in vertical motions does not follow the decline in star light which drops with radius as $\sim \exp^{-\frac{r}{30''}}$. Figure 9 shows that, the broadest profiles seem to be found in relatively low column density areas between the spiral arms (as traced by H I). As such we do not find a correlation between the velocity dispersion of stars in the disk or the H I column density.

The dissimilarity between stars, star-formation, H I intensity, and the kinetic energy in the gas implies that processes other than those directly associated with stars put energy into the ISM. Sellwood & Balbus (1999) suggested that magnetic fields with strengths of a few micro-gauss in these extended disks allow energy to be extracted from galactic differential rotation through MHD-driven turbulence. While that mechanism predicted a uniform dispersion outside of the optical disk, in an attempt to explain lower quality data on NGC 1058, a similar mechanism has the potential of explaining the level and behaviour of the velocity dispersions as a function of radius (Sellwood, private communication). The Sellwood & Balbus (1999) paper generated significant work on numerical models that predict the occurance of the magnetorotational instability in galactic disks (e.g. Dziourkevitch, Elstner, & Rudiger 2004, Pionteck & Ostriker 2004).

5.   Profile Shapes

Any model that would explain how energy is put into the ISM must account for the shape of the profiles in NGC 1058. A single Gaussian least-squares fitting routine was run on the $30''$ and $45''$ data sets. In both cases, we found that while the signal to noise for most profiles was excellent the chisq per degree of freedom was larger than a few, the residuals also suggested that the wings were broader than those of a Gaussian.

To understand whether how the H I line shapes varied throughout the galaxy, the profiles were normalized by flux, aligned so that their peaks were at the same central velocity. These were plotted in units of FWHM ($2.354\sigma_v$), using the parameters from the single Gaussian fits to control the scaling. This was done to reveal only the difference in the line shapes and not other differences such as the width of peak intensity. While stacking up the $45''$ profiles it became clear that almost all profiles appeared to have the same shape. Figure 13 suggests that despite it being non-Gaussian, the shapes of the line profiles are identical throughout most of the galaxy when scaled by σ_v and their peak flux and aligned so that their peaks occur at the same velocity.

For the $45''$ data, median shapes from profiles within different width and peak intensity ranges were compared and found to be identical within the error-bars. The method used to derive such median line shapes is fairly straightforward. After the pixel selection (by FWHM,

location in the galaxy, etc.) the profiles corresponding to every pixel were normalized in intensity dividing by the peak flux. A grid of 63 channels for the $45''$ data and 108 for the $30''$ data was set up to replace the velocity axis from units of km/sec to units of FWHM. For example suppose that the velocity corresponding to the peak of a certain profile (in the $45''$ cube) is $V_{cen} \, \mathrm{km \, s^{-1}}$ and that its FWHM is $FW \, \mathrm{km \ s^{-1}}$. Only the channels between $V_{cen} - 3 \times FW$ and $V_{cen} + 3 \times FW$ were used in deriving the median shape. The normalized fluxes corresponding to these channels were then resampled onto a grid where each bin (i.e.; channel) is $6 \, FW$ divided by the number of channels. Each bin therefore contains a certain number distribution of normalized fluxes; these fluxes were then sorted and the middle value is taken as the median.

Median profiles were also derived and compared from various areas throughout the disk and the line shapes appeared similar everyhwere except in N and S, where the profiles where more asymmetric as previously discussed. For brevity we present just two of these tests in Figure 14. The same median comparison tests were done on the $30''$ data. At the $30''$ resolution median profiles derived for certain ranges of peak flux and from various areas throughout the galaxy were also identical. However, the median profiles derived for various ranges of FWHM appeared to vary in the shape of their wings, perhaps because of the lower signal to noise in this data set, and to the smaller number of broad ($\sigma_v \geq 10 km \ s^{-1}$) than that of narrow lines.

Throughout our analysis we assumed that the noise characteristic in each profile is random and that the rms noise is the same regardless of the strengh of the signal. This assumption need not be true as deconvolution algorithms seem to produce noise that is proportional in a non-linear fashion with signal (Rupen 97). However different noise for different flux levels will hardly lead to a universal, non-Gaussian line shape. A double Gaussian (a narrow and a broad component) as shown in Figure 15 is a good fit to the median profile derived from the $45''$ data.

6.   Kinetic Energy Distribution

The uniformity of the profile shape in NGC 1058 suggests that on scales of 2.5 kpc, the neutral gas is being stirred into the same distribution of energy per unit mass and that this distribution is different than that for other galaxies (e.g. the Milky Way). Figure 16 shows the normalized kinetic energy (KE) distribution for the Milky Way and for NGC 1058. This comparison is only qualitative. The term "normalized" in the case of the Milky Way refers to the fact that the KE distribution was obtained from a model (i.e. double Gaussian fit) of the H I emission at the North Galactic Pole; this model was presented in Kulkarni

& Fich (1985), hereafter KF85, and it only includes "normal" emission, i.e. it does not include emission from the H I falling into the disk. These authors corrected for the infalling emission by assuming that the huge bump on one side of the profile represented infalling gas. To remove the bump they reflected the profile about the velocity corresponding to the peak flux and obtained the profile shown in Figure 16. The units of the KF plot are Kelvin^2 km^2 s^{-2}. The units for the NGC 1058 are arbitrary, and the term "normalized" in this case means that instead of flux or temperature, we use flux divided by peak flux, and bin numbers instead of velocities. To compare those qualitatively we aligned the KF profile with the NGC 1058 median profile from the entire 45″ data set. The aligning was done by fitting a single Gaussian to the KF85 profile and to the NGC 1058 median profile. We require and that the limits of the KF85 and the NGC 1058 profiles span an equal number of FWHM.

The striking feature in the Galactic energy distribution, also noted by Kulkarni & Fich (1985) is the almost constant kinetic energy for about 50 km/sec. In contrast, NGC 1058's KE curve is more centrally peaked. Presumably the KE distribution is set both by the galactic potential as well as explosive ISM events (such as SNe, star formation, and infalling gas). It is not perfectly clear how these factors have shaped the energy distribution as a function of velocity of either the Milky Way or NGC 1058. function of velocity.

7.   Beam Smearing and Bulk Motions

An accurate study of the profile shapes throughout the galaxy require us to understand the effect of beam smearing on our measurements. Consider a round spiral disk with gas moving in circular orbits at a velocity v_{circ}; attaching polar coordinates to this disk (r_d, θ) and letting the angle between the normal to the plane of the galaxy and line-of sight be referred to as the inclination angle (i) the observed radial velocity on a set of sky-coordinates (x, y) will be

$$v_z(x, y) = v_z(r_d, \theta)cos(i) + v_{circ}(r_d)\ sin(i)cos(\theta) + v_{red}$$

where v_{red} is the velocity of the galaxy for which with respect to the observer. Obviuosly a smaller i is (a more face-on) makes it easier to measure the true v_z distribution. A gradient in the $v_{circ}(r_d)sin(i)cos(\theta)$ across the resolution element (beam) will increase the width of the profile and confuse the measurements of the velocities perpendicular to the disk. This problem is known as beam smearing.

Two tests were performed using our highest resolution (15″) data to quantify the effect of beam smearing on our measurements of σ_v. First, we determined the maximum in-plane velocity difference within a beam which would contribute to the width of the line profile at a certain position in the galaxy (i.e. at a pixel). This was done by finding the maximum

difference (hereafter M_{diff}) between the central velocity v_{cen} (i.e. the velocity associated with the peak flux as derived from the single Gaussian fit to the $15''$ data) of the H I pixel and the central velocities of all the pixels within a square with $32''$ sides centered on that pixel. Figure 11 shows the map of these maximum difference. This method is based on the assumption that differences in v_{cen} are due to gas motions in the plane of the galaxy. This test shows that σ_v is correlated with M_{diff}. The correlation between σ_v and M_{diff} suggests the exitence of bulk motions on scales smaller and equal to those probed by our highest resolution data $15''$ (0.7 kpc).

Finding M_{diff} across NGC 1058's disk gives an upper limit to the broadening of the H I profiles. To better understand the effect of beam smearing on our observations we constructed a simple model of how H I in NGC 1058 would appear if it was an infinitely cold disk; we then convolved this model with a $30''$ beam and ran our Gaussian least squares fitting routine on the resulting H I profiles. The widths of these final model profiles were significantly smaller than those measured in NGC 1058 (Figure 12) suggesting that beam smearing does not have a significant impact on our observations.

8. Summary and Conclusions

Excellent resolution and high sensitivity H I observations of NGC 1058 show an intriguing picture of the interstellar medium throughout this galaxy: the velocity dispersion ranges from 4 to 14 km/sec but is not correlated with star formation or the spiral arms, which is another major ISM regulator. Global trends such as a radial fall-off must be explained in the context of significant local effects; most notable among these are isolated, resolved regions of high velocity dispersions as well as significant scatter in the dispersion at a given radius. In summary unlike some previous studies, we find that the dispersion is not constant and it does not simply decline with radius. we also find that there is no tight correlation between the width of the profiles and the spiral arms.

The most probable source for the highest dispersions observed outside the central regions are small scale ($\leq$0.7 kpc) bulk motions. The energy sources supporting such motions are not entirely clear. The disk is warped in the southern part (van der Kruit & Shostak 1984, Shen & Sellwood 2006), leading to the observed broad profiles: however, a similar explanation for region N would suggest a rather impressive small-scale structure in the warp, as it would require the inclination to change by ~ 3 degrees over a size smaller than 0.7 kpc.

There is no obvious correlation with stars or star formation tracers such as Hα, radio continuum, SNe except in region C; nor is it clear what role, if any, is played by spiral arms

in driving the observed small scale bulk motions. Some of the measured velocity dispersions are higher than the 10 km s^{-1} canonical sound speed in the ISM, but since we cannot easily measure directly the pressure and 3-dimensional density structure of the gas, we cannot determine the exact sound speed to know if we are indeed seeing supersonic motions.

The shapes of the H I profiles in NGC 1058 are non-Gaussian and hence cannot be explained as emission from single temperature gas. Therefore, it is not clear whether these narrow profiles are evidence of a lower thermal balance point between heating and cooling mechanisms in NGC 1058's outskirts as compared to the rest of the galaxy.

A double Gaussian description of the H I profile is far from a complete surprise. The surprise is the constancy between the broad and narrow components throughout NGC 1058's H I disk. In previous studies (e.g. Mebold 1972, Young & Lo 1996) it was found that some of the H I profiles were well described by double Gaussians, and these associated the narrow Gaussians with the CNM and the broad with the WNM. Young & Lo (1996) found that the narrow component existed only in regions of high H I column density, next to areas with active star formation. It is unlikely that the universal profile in NGC 1058 can be explained as a combination of cold and warm medium for the narrow and broad component respectively, because it seems difficult to have the same ratio of warm to cold gas in regions associated with stars and star fromation and at radii three times the optical R_{25}. Also, high resolution observations in other galaxies (Braun 1998) showed that the CNM dissappears at the edges of the optical disk.

Further quests on the observational front such as (at what resolution will this universality break down, is this spatial scale particular to NGC 1058, can we see the same shape and/or its universality in other systems), as well as theoretical efforts to model mechanisms of injecting energy into the ISM, and determine how that energy dissipates throughout a fractal ISM are necessary to understand the full significance of the universal profile in our 45″ data cube.

REFERENCES

Allen, R. J., and Shostak, G. S. 1979, Astron. Astrophys. Suppl. 35, 163

Braun, R. and Walterbros R. A. M. , 1992 ApJ, 386, 120

Braun, R., 1997 ApJ484, 637

Braun, R., astro-ph/9804320 Interstellar Turbulence, Proceedings of the 2nd Guillermo Haro
    Conference. Edited by Jose Franco and Alberto Carraminana. Cambridge University
    Press, 1999., p.12

Dickey, J.M. and Lockman, F.J., 1990, Annu. Rev. Astron. Astrophys. 28, 215

Dickey, J.M., Mebold, U., Stanimirovic, S., Staveley-Smith L., 2000, ApJ, 536. 756D

Dziourkevitch, N., Elstner, D., & Rudiger, G., 2004, A& A, 423, L29

Eskridge, P. B., Frogel, J. A., Pogge, R. W., Quillen, A. C., et al. 2002, ApJS, 143, 73

Ferguson, A., Wyse, R. F. G., Gallagher, J.S., Hunter, D.A., 1998 ApJ506, 19

Ferguson, A., Gallagher, J. S., Wyse, R. F. G., AJ, 116, 673

Kulkarni, S.R. and Fich, M., 1985 ApJ289, 792

Kulkarni, S.R. and Heiles, C., 1988 in Galactic and Extragalactic Radio Astronomy, ed. G.L.
    Verschuur& K. I. Kellermann (New York: Springer Verlag), 95

Lewis, B.M., 1984 ApJ285, 453

Lewis, B.M., 1987 ApJS63, 515

Lewis, B.M., 1987 Obs. 107, 201L

Li, Y., Mac Low, M.M., & Klessen, R.S., 2005, ApJ, 620, L19

Lockman, F. J., 1984, ApJ, 283, 90

Lockman, F. J. and Gehman, C. S., 1991, ApJ, 382, 182

Mac Low, M.M., & Klessen, R. S., 2004, Rev. Mod. Phys. 76, 125

Malhotra, S., 1994, ApJ, 433, 687

Malhotra, S., 1995 ApJ, 448, 132

McKee, C.F.,Ostriker, J.P. 1977, ApJ, 218, 148

Mebold, U., 1972, A& A, 19, 13

Merrifield, M. R., 1993, MNRAS, 261, 233

Olling, R., 1995, PhD Thesis

Olling, R., 1996, AJ 112, 457

Oort, J. H., 1932, Bull. Astron. Inst. Netherlands, 6, 349

Piontek, R. A., & Ostriker, E. C., 2004, ApJ 601, 905

van der Kruit, P.C., Shostak, G.S., 1982 A&A, 115, 293S

Rupen, M. P., 1987 PhD thesis

Rupen, M. P., 1997, VLA Scientific Memorandum, No. 172: A Test of the CS (Shortened C) Configuration available at http://www.vla.nrao.edu/memos/sci

Rupen, M. P., 1998, VLA Scientific Memorandum, No. 172: A Test of the CS (Shortened C) Configuration available at http://www.vla.nrao.edu/memos/sci/175/cstest2/

Rupen, M.P., 1999, *Spectral Line Observing II: Calibration and Analysis* in ASP Conf. Ser.,180, Synthesis Imaging in Radio Astronomy II ed. by Taylor, G.B., Carilli, C.L., & Perley, R.A. pg. 229

van der Kruit, P.C., Shostak, G.S., 1984 A&A, 134, 258V

Shen, J. & Sellwood, J. A., MNRAS, 2006 370, 2

Sellwood, J. A. & Balbus, S.A., ApJ 1999, 511, 660

Shostak, G.S., van der Kruit, P.C., 1984 A&A, 132, 20S

Young, L.M., Lo, K.Y. 1996 ApJ, 462, 203

Young, L.M., Lo, K.Y. 1997 ApJ, 476, 127

Young, L.M., Lo, K.Y. 1997 ApJ, 490, 710

Table 1.   General Properties

NGC 1058	
R.A.(B1950)	02 40 23.2
Dec (B1950)	+37 07 48.0
Morphological type	Sc
V_{sys} [km/sec]	518
L_B [$L_\odot$]	1.5×10^9
M_{HI}[$M_\odot$]	2.3×10^9
SFR [$M_\odot \, yr^{-1}$][a]	3.5×10^{-2}
$D_{25} \times d_{25}$ [arcmin][b]	3.0×2.8
Distance[Mpc][c]	10
Physical equivalent of $1''$	$48.5 \, pc$
Inclination[d]	4–$11°$
Environment[e]	member of the NGC 1023 Group

[a]SFR stands for Star Formation Rate, it was calculated from Hα fluxes by Ferguson, Gallagher & Wyse (1998)

[b]NASA/IPAC extragalactic database (NED)

[c]Ferguson, Gallager, & Wyse (1998)

[d]van der Kruit & Shostak (1984)

[e] Lewis (1975)
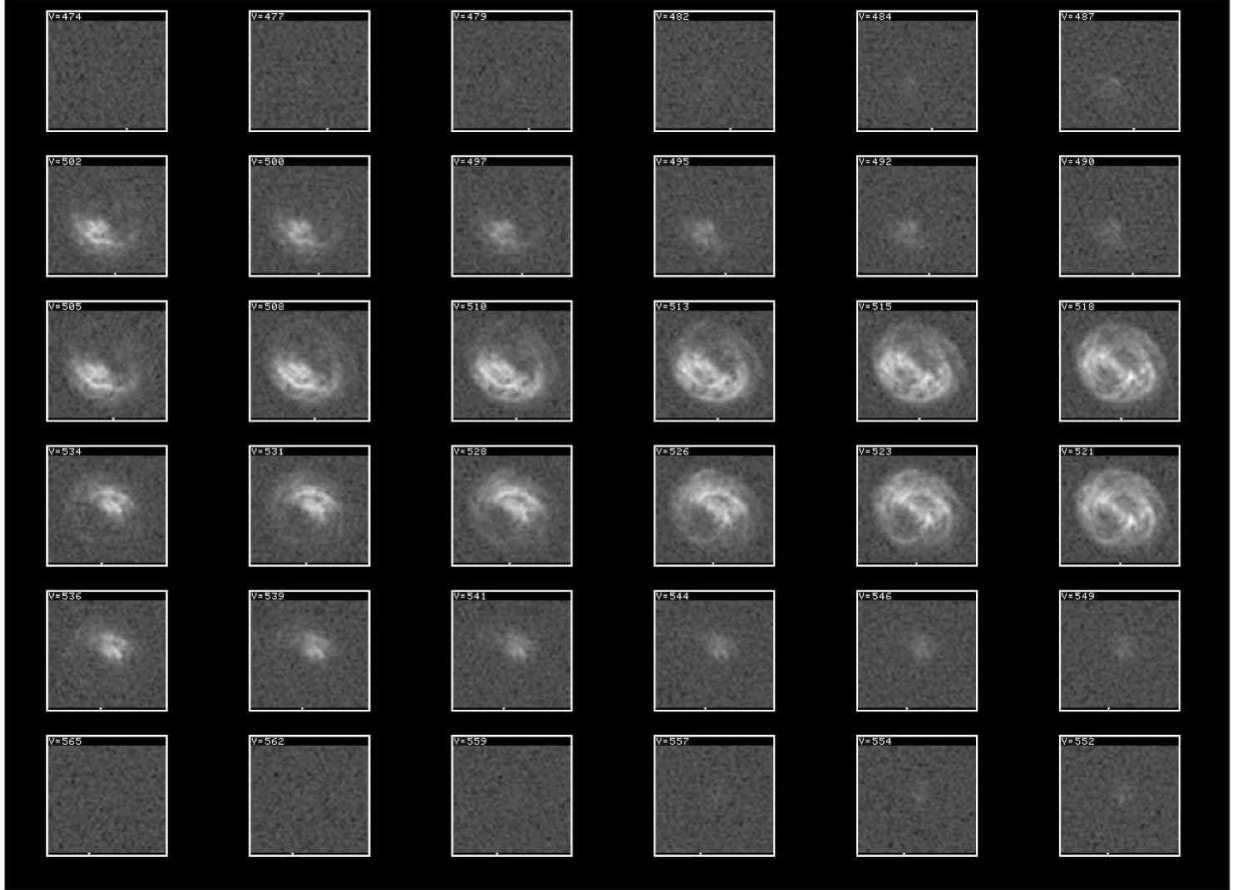
Fig. 1.— Sample channel maps for NGC 1058–Each square image represents the H I 21 cm line emission within a velocity range of $2.58\,\mathrm{km\,s^{-1}}$ where the central velocity of that range is given on the upper left corner of each image. The x and y axis of every channel map gives the Right Ascension (RA) and Declination (Dec) coordinates,and are identical to these in Figure 2. Such sample channel maps can be assembled together in the same way the frames of a movie are put together to make what is refered to as a data cube.
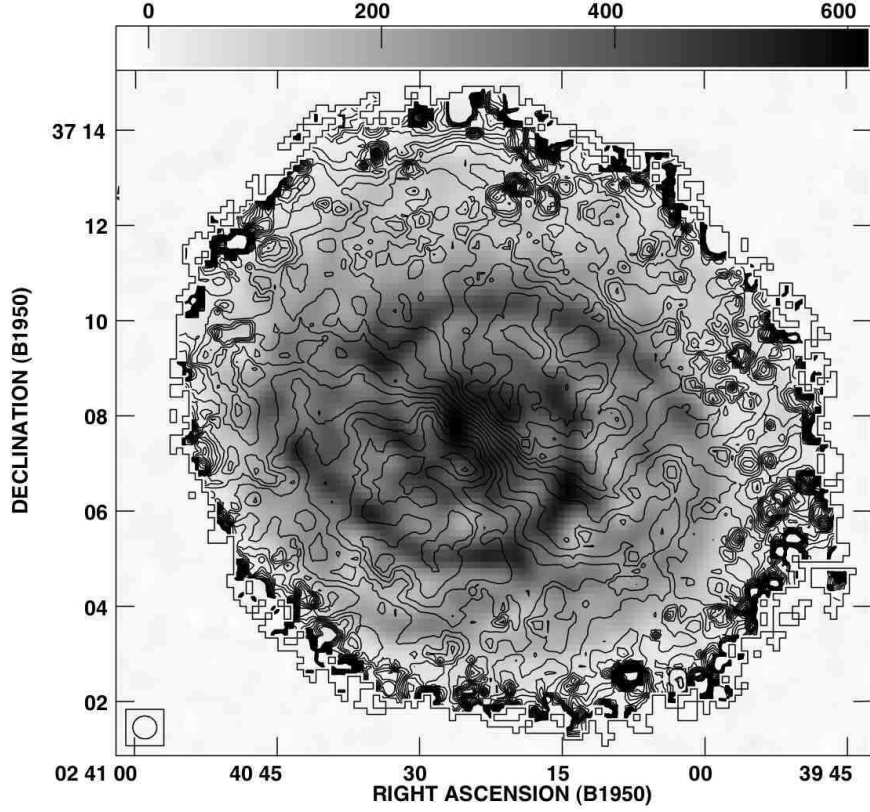
Fig. 2.— Intensity weighted mean velocity contours atop H I intensity map for NGC 1058
Intensity weighted mean velocity contours atop H I intensity map (grey) for NGC 1058—This
figure was made using the 15″ data cube with a sensitivity of 0.5 mJy/beam corresponding
to a column density of 1.6×10^{18} cm^{-2}. The physical resolution of this image is 0.7 kpc and
the velocity contours range between 500 and 558 km/sec in 2 km/sec increments. The H I
disk in NGC 1058 extends to a diameter of more than 20 kpc.
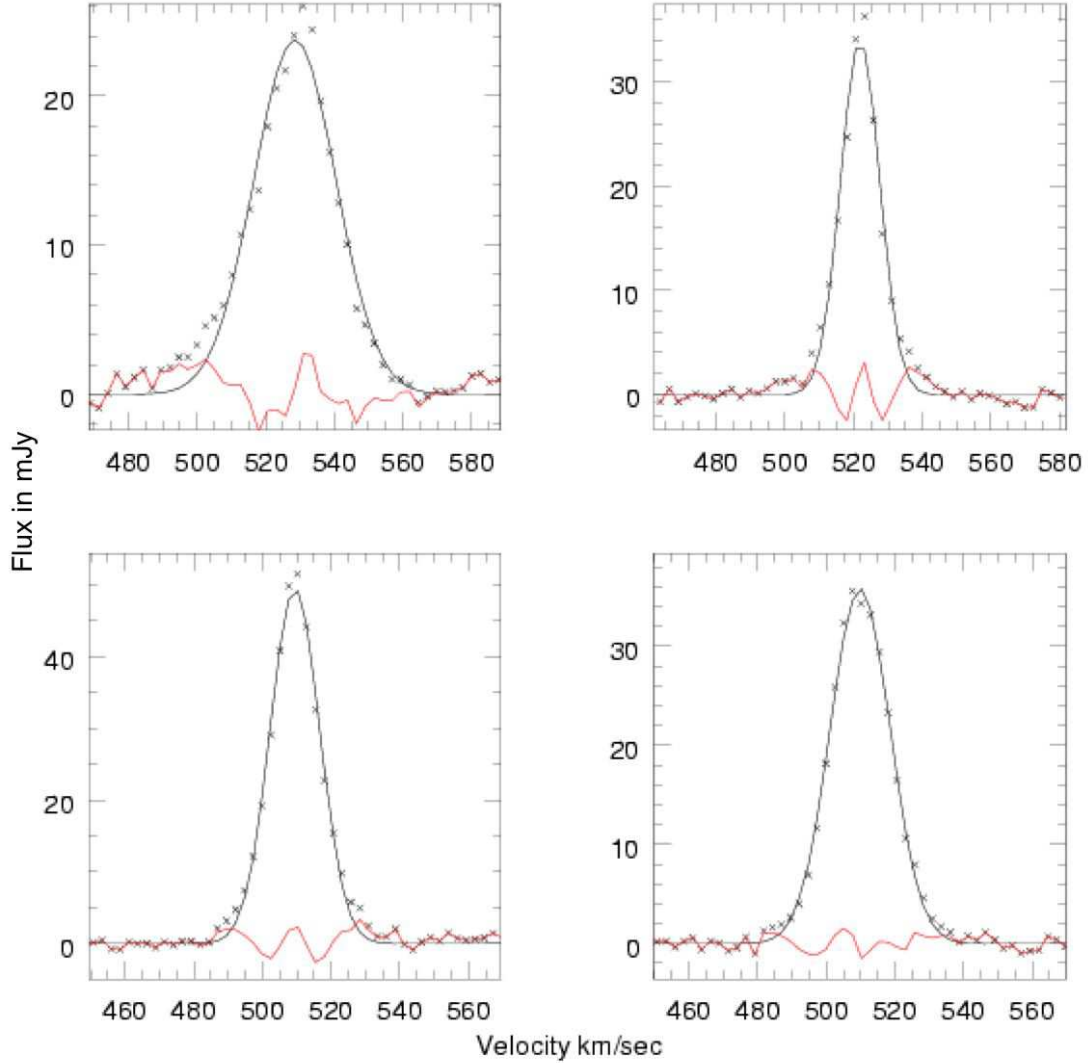
Fig. 3.— Four sample of H I profiles (crosses), the Gaussian fit (solid line) and the residual pattern (red) with σ_v from the Gaussian fit: 12.7 km/sec (upper left, pixel from a region of high dispersion), 5.95 km/sec (upper right, pixel from a region of low dispersion), 7.6 km/sec (lower left pixel from an interarm region), 9.3 km/sec (lower right, pixel from an arm region). The x axis is in km/sec and the y axis represents H I intensity in mJy/beam. The shown residuals indicate that a single Gaussian function does not adequately describe the line shapes. However the width of the Gaussian does track the breadth of the H I profile. This figure is based on the $45''$ data cube and the single Gaussian fits done for that cube.
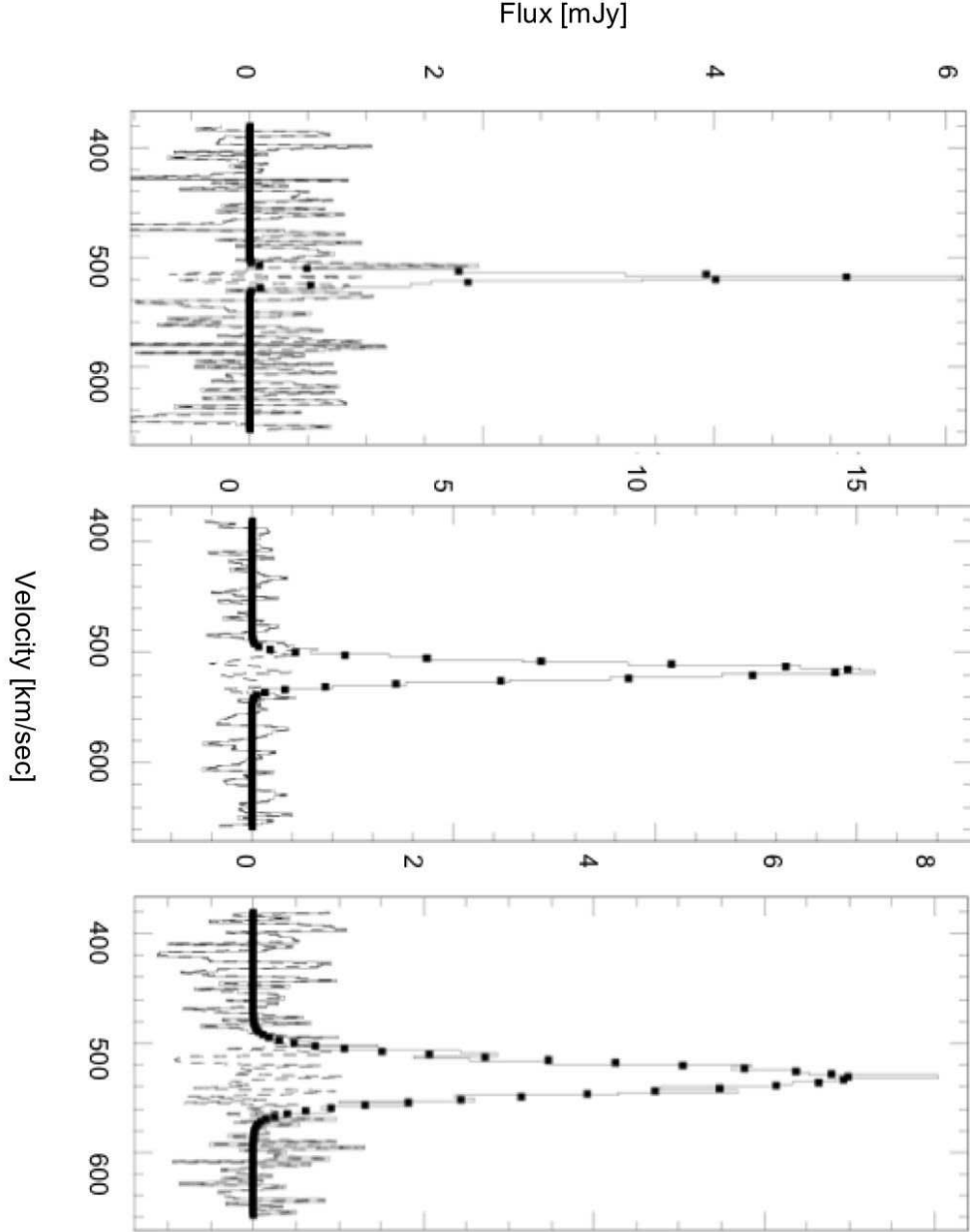
Fig. 4.— Three samples of H I profiles (solid line), the Gaussian fit (squares) and the residual pattern (dashed) with σ_v from the Gaussian fit: 3.8, 7.6, and 13.2 respectively. Figure based on the $30''$ data cube and the single Gaussian fits done for that cube. The x axis is in km/sec and the y axis represents H I intensity in mJy/beam.
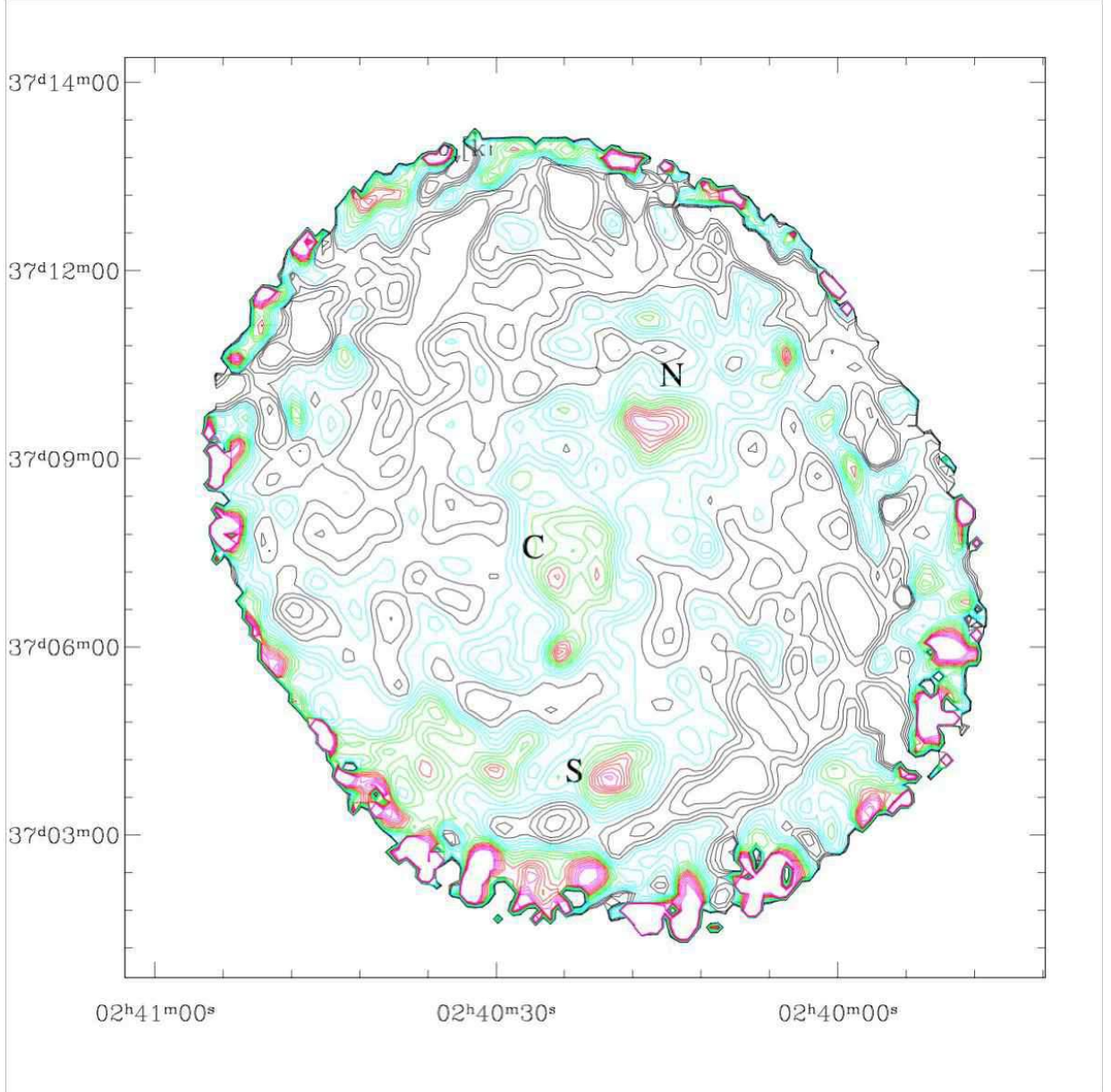
Fig. 5.— Distribution of dispersions throughout NGC 1058; the regions of highest dispersion are labeled N, C, and S. The x and y axis are the RA and Dec in B1950 coordinates. This figure is based on the results of the single Gaussian fit performed on the 30″ data. The contours are in km/sec and start in steps of 0.5 km/sec. Black is used for dispersions between 5.5 to 7, cyan for 7.5 to 9, green for 9.5 to 11, red for 11.5 to 13, and magenta for 13.5 to 15 km/sec.
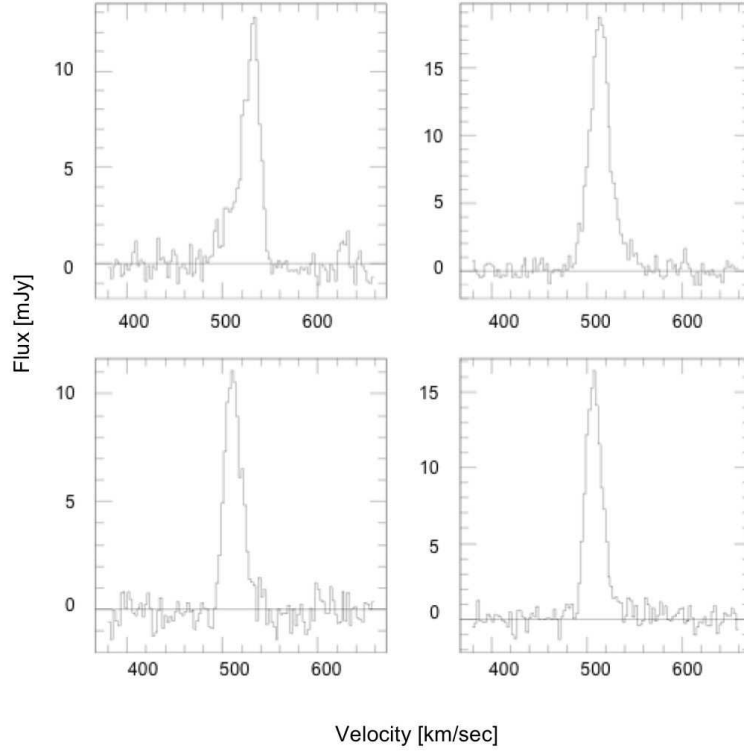
Fig. 6.— Four sample profiles in the regions with highest asymmetries (of order few percent); The x axis of each of the four plots represents velocity and is in units of km s^{-1} and the y axis represents H I intensity in mJy/beam, where the beam refers to the point spread function of the observations. The upper left is from region N, upper right from C, lower left from S, and lower right from a region West of S. Regions N,C, and S are shown and labeled in Figure 3.
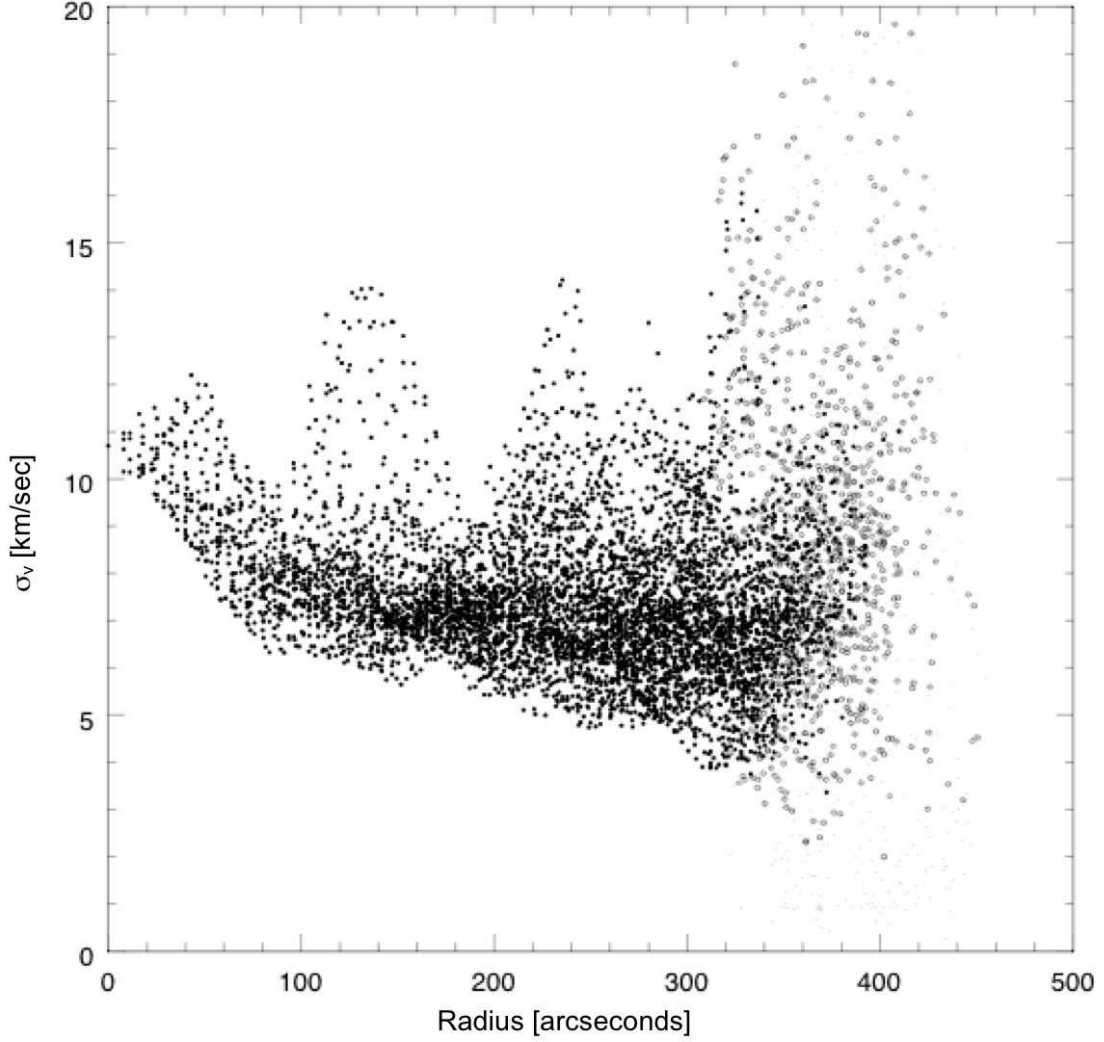
Fig. 7.— Radial dependece of NGC 1058's σ_vs—The x axis (in arcseconds) gives the radius while the y axis (in km/sec) gives the σ_v as derived from single Gaussian least squares fits to the 30″ data cube. The filled circles represent points with error bars,less than 12.5% of σ_v, the empty circles – points with error bars between 12.5% and 25% and the dots– points with errors greater than 25%. Despite a few high σ_v regions (N,S in Figure 5, the radial falloff is evident.
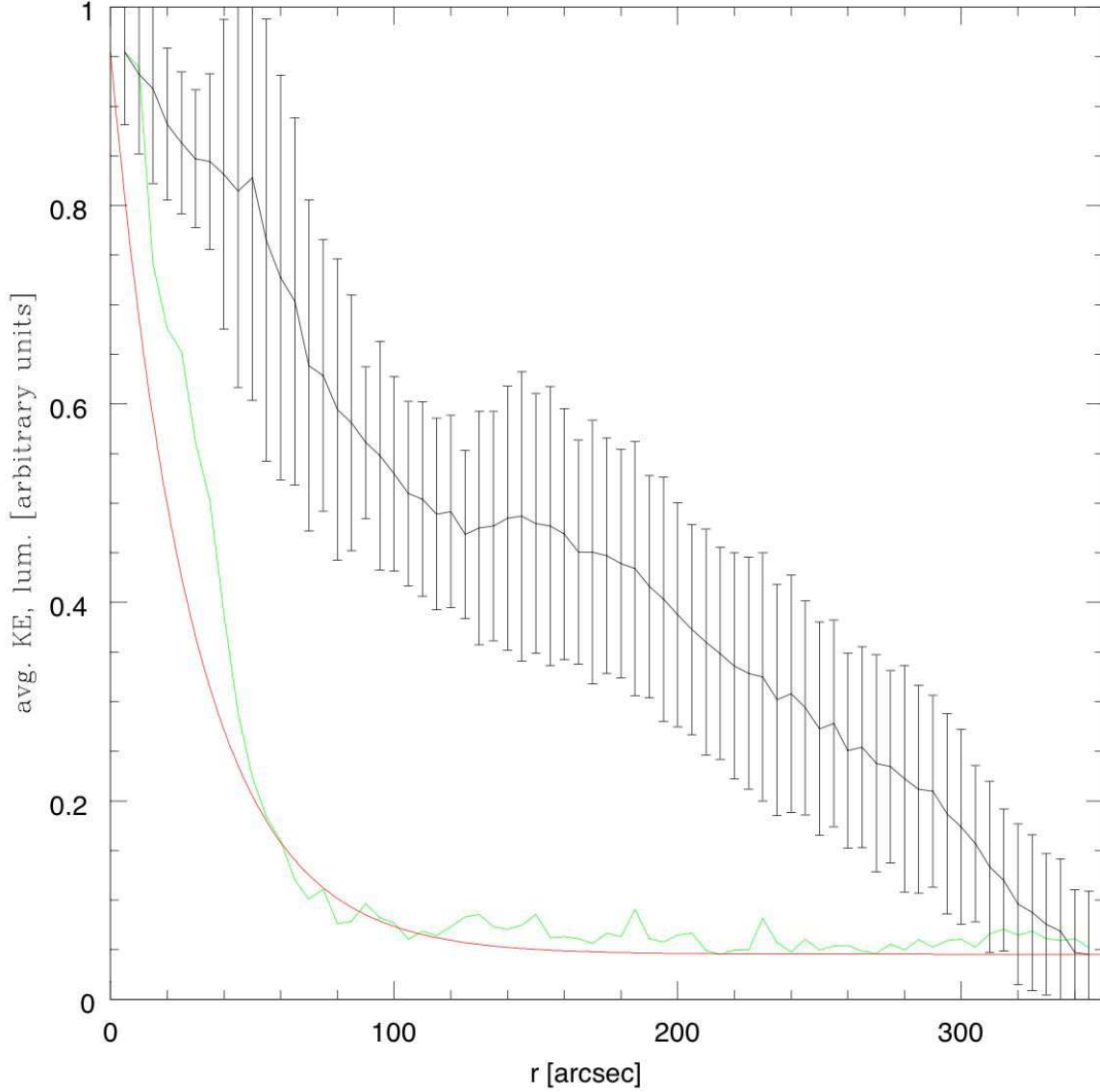
Fig. 8.— The energy in the neutral gas was roughly approximated as the product of the total H I intensity and the square of the velocity dispersion. Both the green and the black lines represent azimuthal averages of concentric rings around the center of NGC 1058. The black error bars show the rms in each of these rings. The red line shows the exponential fit to the stellar data. The energy in the gas falls off with radius much slower than the stellar luminosity suggesting that processes other than those associated with star input energy are responsible for heating the gas at large radiae.
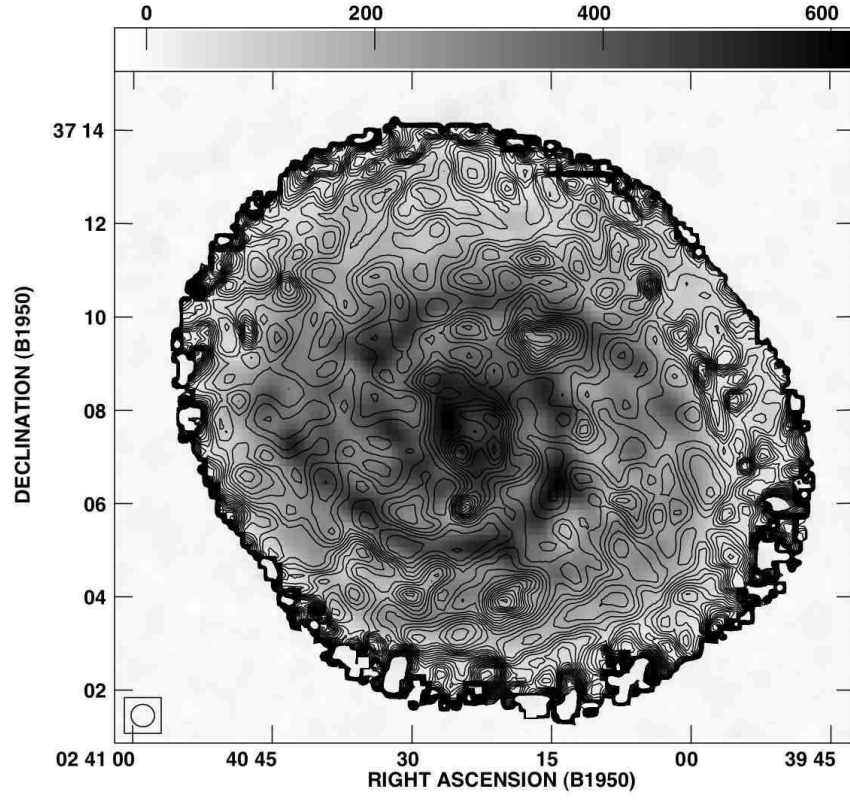
Fig. 9.— σ_v contours atop of an H I total intensity map—The contours range from 4 to 14 km/sec in steps of 0.5 km/sec and are based on the single Gaussian fit to the $30''$, NGC 1058 data cube. Note that regions N and S of high σ_v are located in the inter-arms.
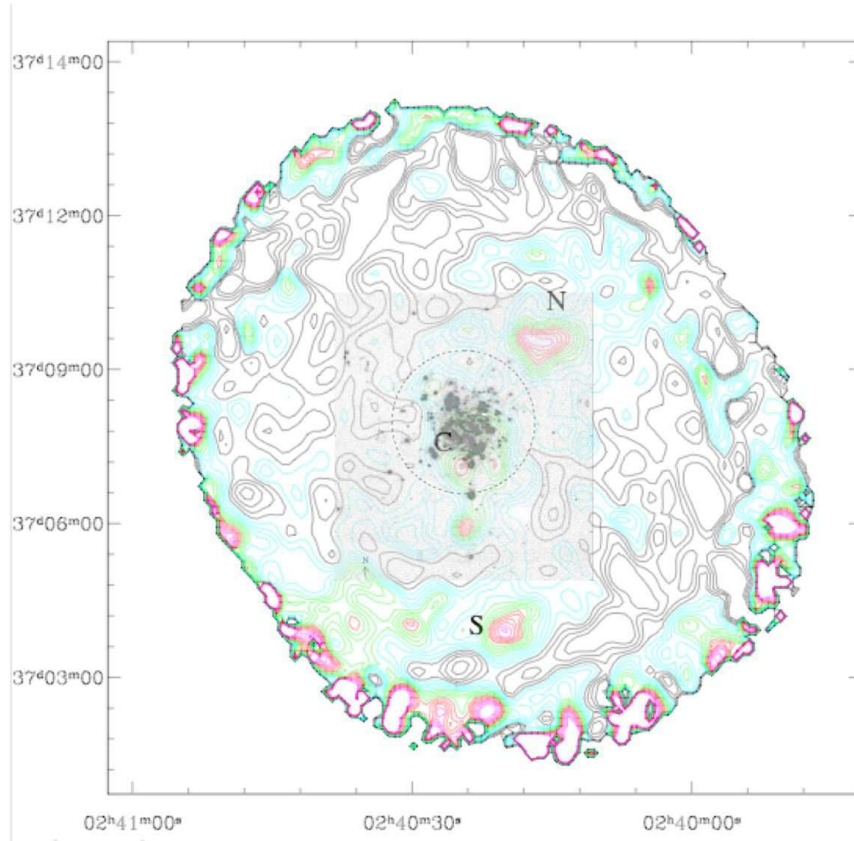
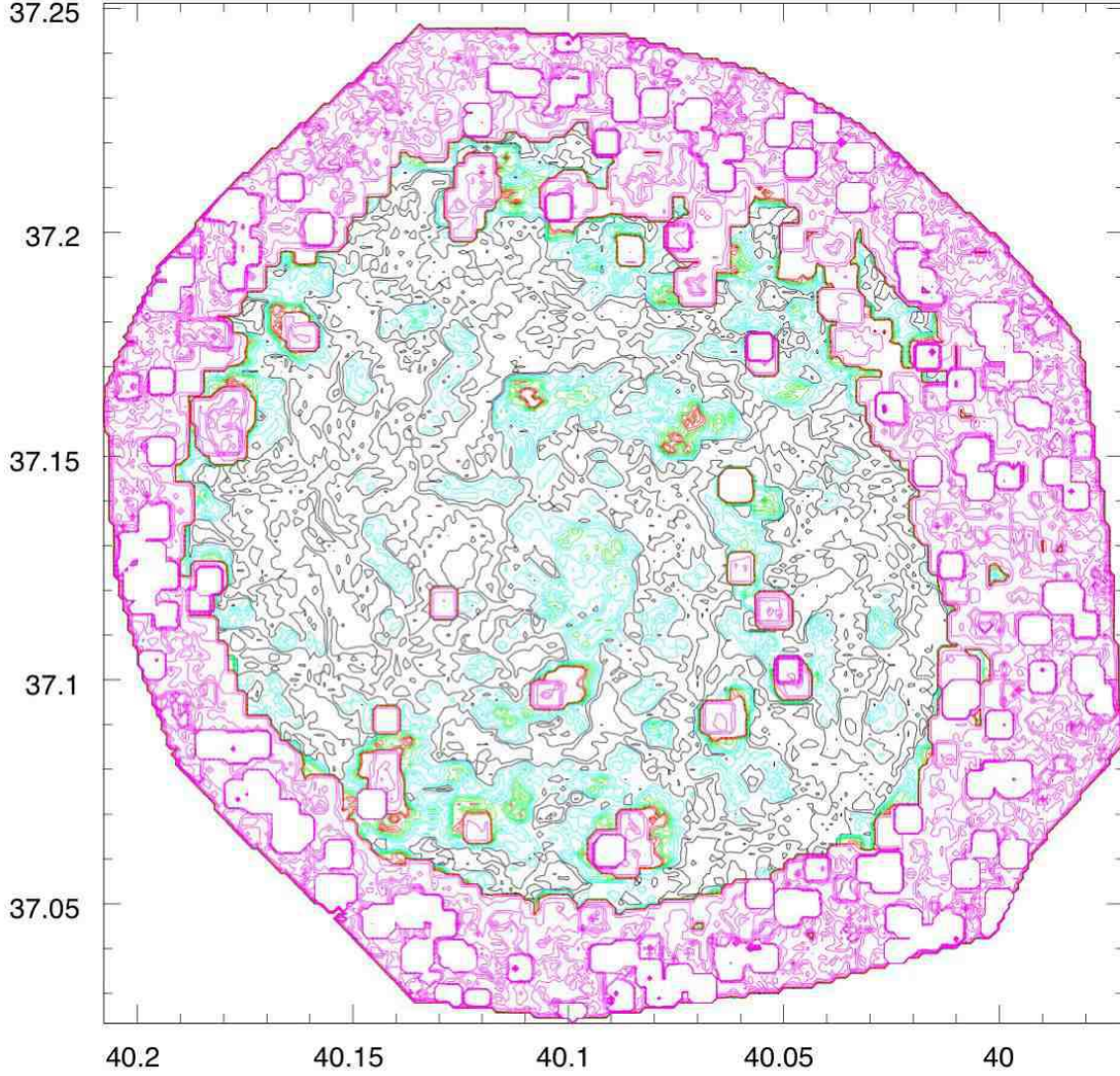Fig. 10.— H$_\alpha$ greyscale from Ferguson, Gallager, & Wyse 1998, atop dispersion contours as in Figure 5.

Fig. 11.— Contours of maximum potential beam smearing in km s^{-1}. Black is used for dispersions maximum beam smearing effect of 1, 2, and 3 km/sec, cyan for 4,5,6, green for 7,8,9, red for 10, 11, and 12, and magenta for values of 30 km/sec and above. 5.5 to 7, cyan for 7.5 to 9, green for 9.5 to 11, red for 11.5 to 13, and magenta for 13.5 to 15 km/sec. The magenta contours are regions where the H I emssion was very faint or non-existent. As such the Gaussian fitting routine employed produced spurious results. The square shape of some of the contours is an artifact of the method employed in determining the maximum beam smearing. This figure is based on the 15″ data cube. Note that the highest velocity gradients are found in regions N and S and south-west of C. Regions N, S, and C are shown and labeled in Figure 5.
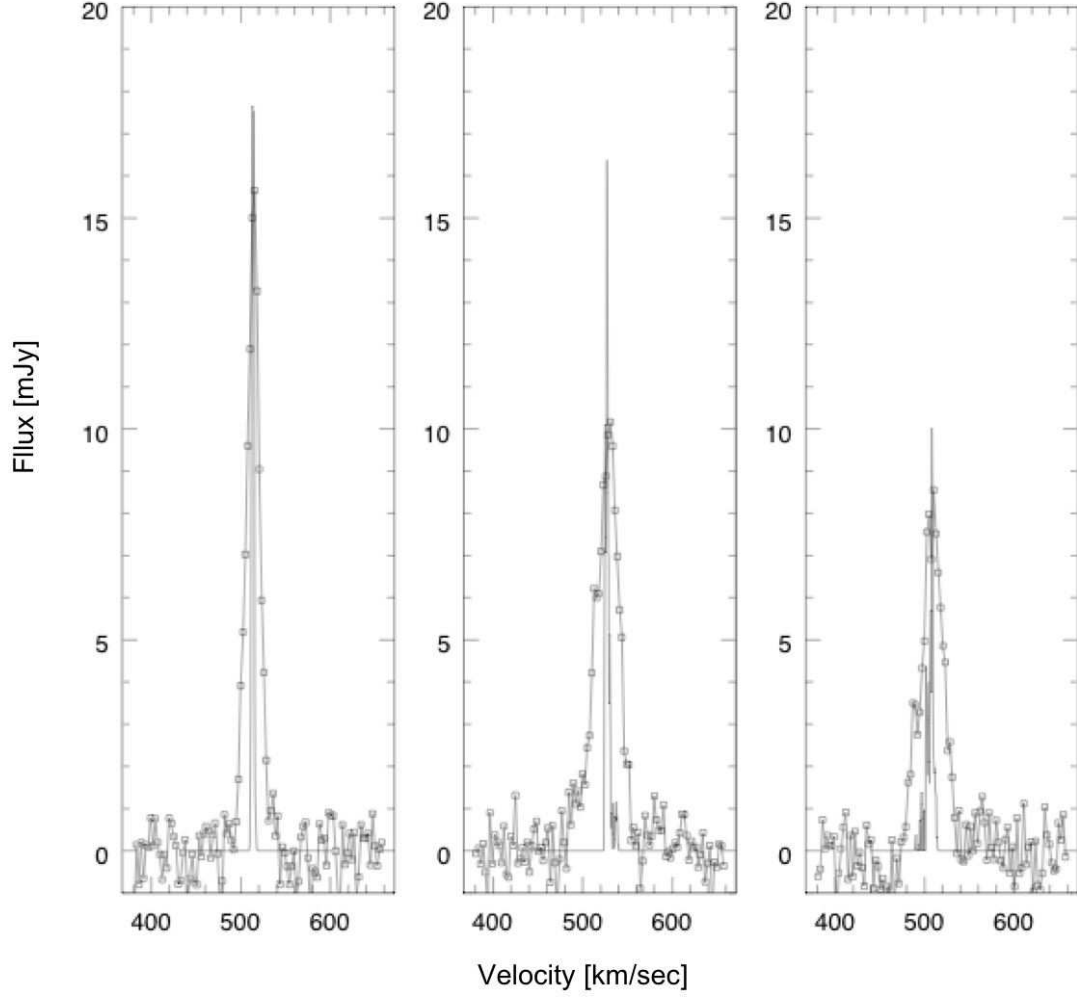
Fig. 12.— Effect of beam smearing on σ_v measurements at $30''$ resolution. The x axis in in km/sec and the y axis is in mJy/beam. The connected squares represent the observed profile. The narrow profiles were obtained by modeling the velocity profiles associated with an infinitely cold disk and then convolving that model with a $30''$ beam, and running the Gaussian least squares fitting routine on the convolved cube.
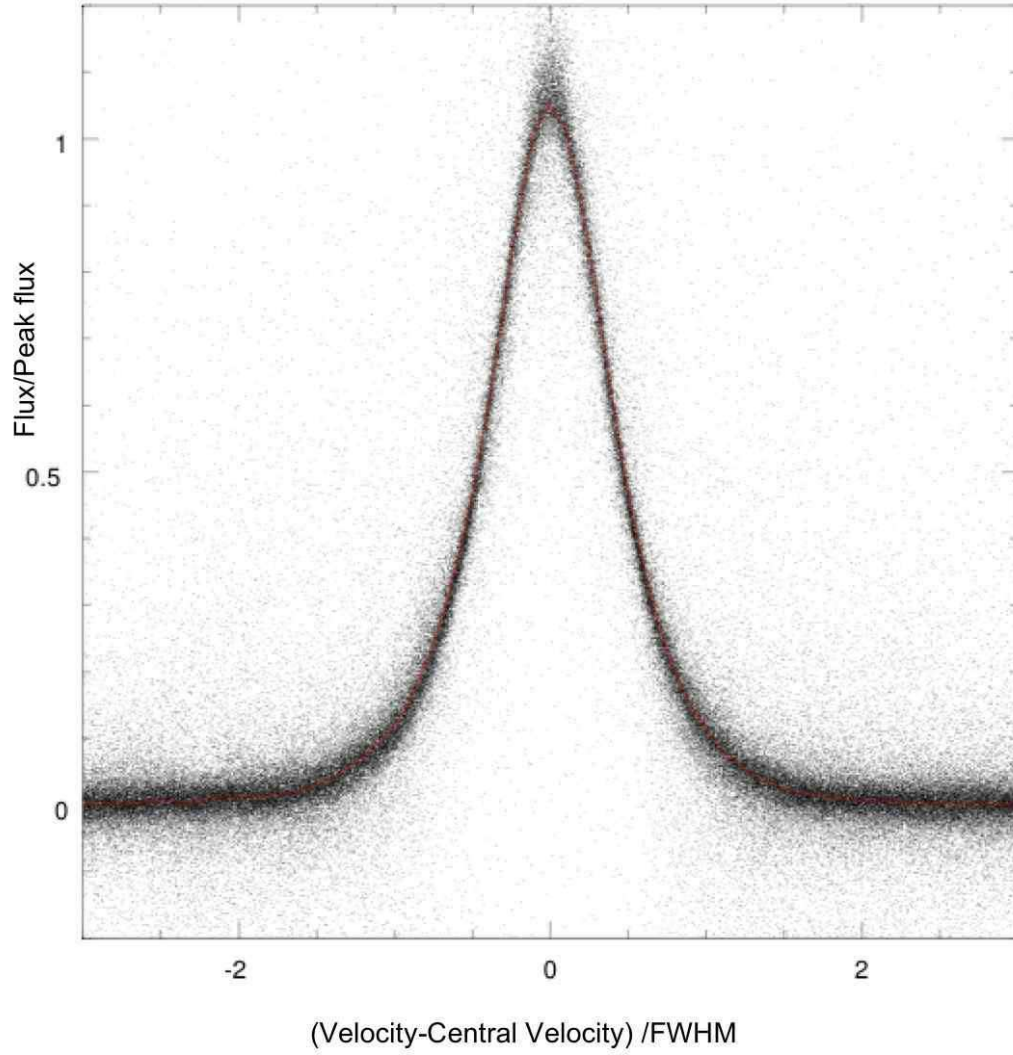
Fig. 13.— Median Profile (red) atop all H I profiles from NGC 1058 45″ data cube. The x axis is flux/peak flux and the y axis is velocity minus the central velocity and divided by the FWHM.
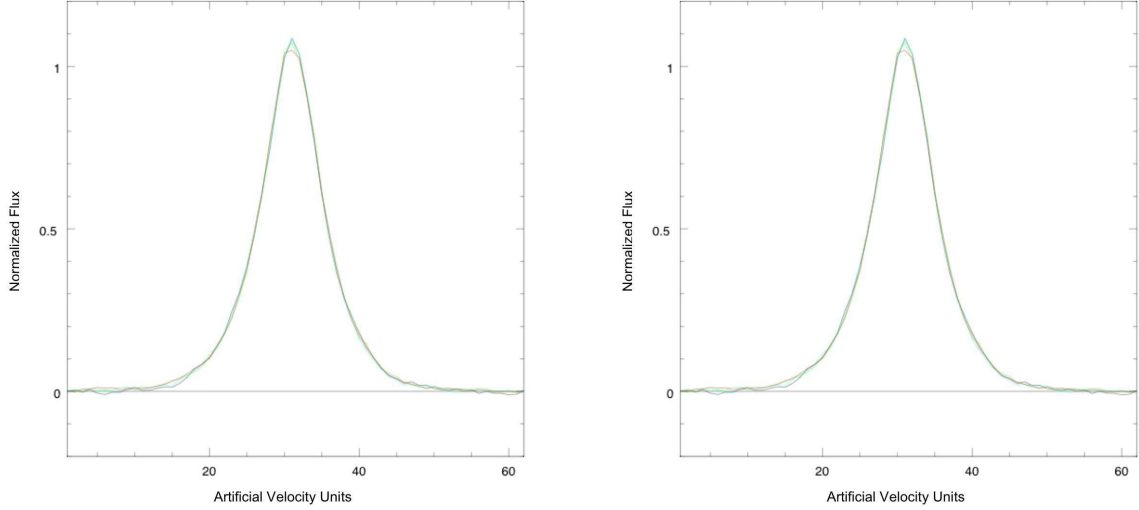
Fig. 14.— Median profiles derived for certain FWHM ranges (left pannel);and for peak flux ranges (right pannel) from the 45″ NGC 1058 data set. The x axis is not in [km/sec] but represents the grid (bin number) on which the profiles were set. Please refer to text for a detailed explanation. The y axis is the flux divided by peak flux. In the left pannel black is used for median profiles with widths (FWHM) between 14 to 18 km/sec, cyan for 18 to 22 km/sec, green 22 and red for 26 to 30 km/sec. In the right pannel a solid line is used for profiles with peak fluxes between 10 and 25 mJy/beam, a dotted line is used for profiles with peaks between 25 and 40 mJy/beam, short dash for 40 to 55, and long dash for 55 to 70 mJy/beam.
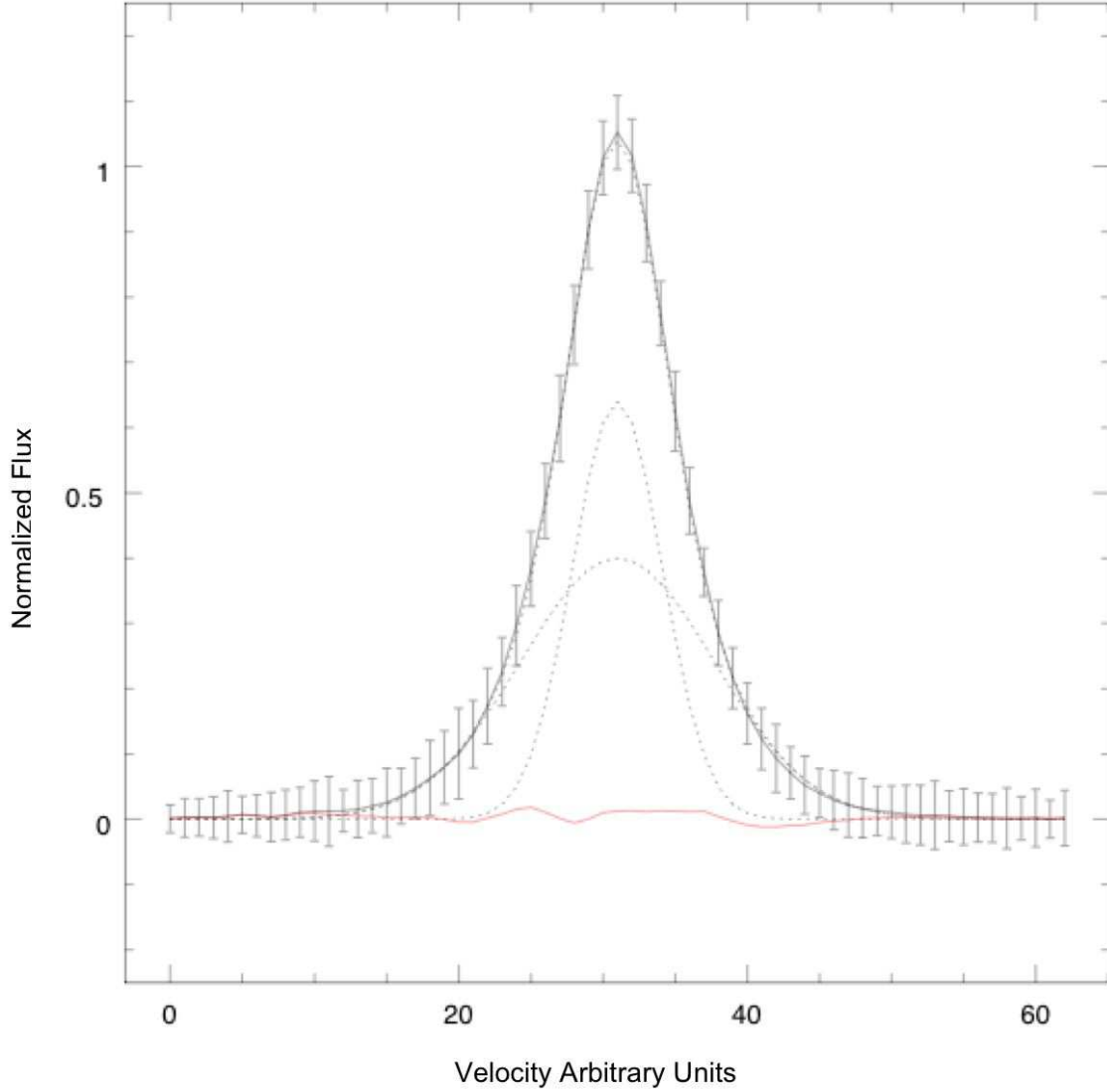
Fig. 15.— Double Gaussian Fit to the Universal Profile — The x axis is in bins as described in the text and the y axis is the flux normalized to the peak intensity. The two Gaussian components used to fit the Median profile and their sum are shown in dotted lines. The residuals are shown in red. Error bars based on the rms in each bin are also given. The ratio between the areas of the broad and narrow components is 1.35 while that between their FWHM is 2.09.
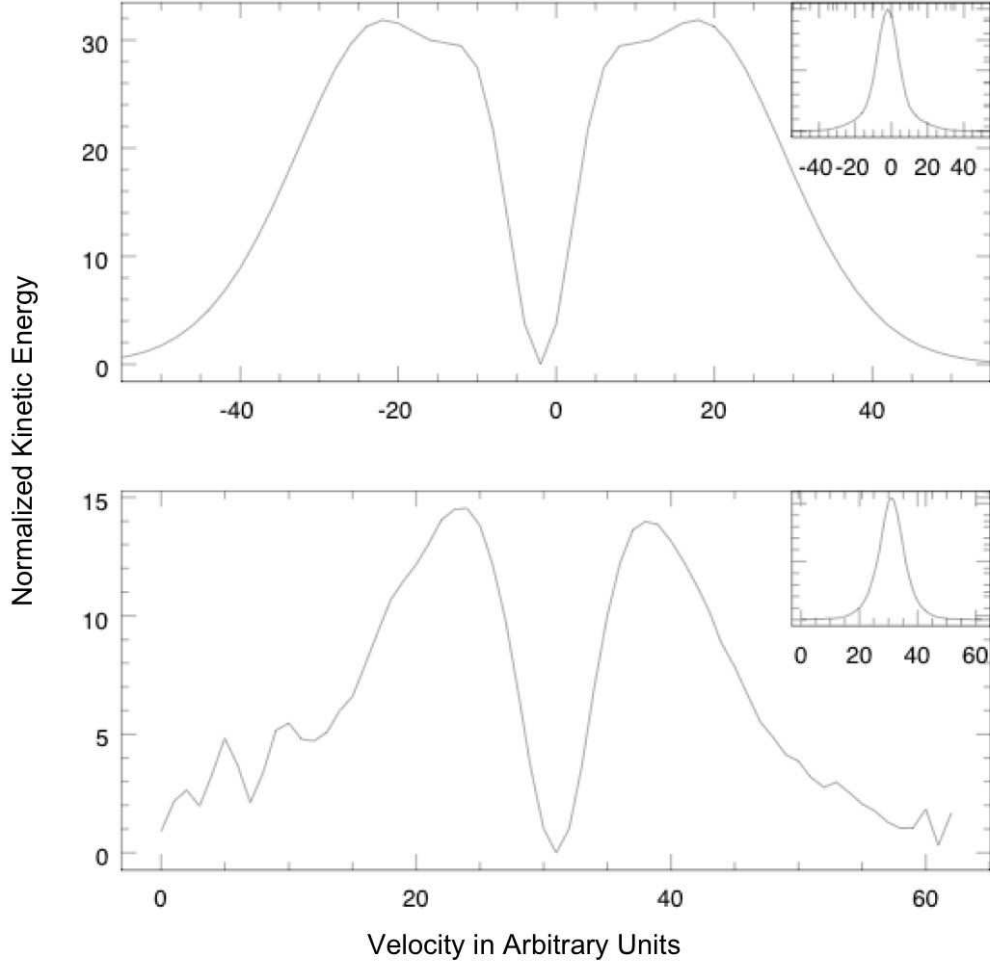
Fig. 16.— Normalized Kinetic Energy distributions for the Milky Way (top) and NGC 1058 (bottom) and corresponding H I profiles. The top figure was obtained from a double Gaussian decomposition of the North Galactic Pole H I emission, from Kulkarni & Fich (1985). For the top figure, the x axis represents velocity in units of $km \, s^{-1}$ and the y axis is the normalized energy in units of Kelvin $km^2 \, s^{-2}$. The inset upper right figure shows the H I profile from which the normalized energy curve for the Milky Way's North Galactic Pole emission was estimated. The bottom figure shows the qualitative behaviour of the kinetic energy distribution with velocity in NGC 1058. Here the x axis represents a bin number (ref.to text) while the y axis represents the qualitative behaviour of the kinetic energy distribution in NGC 1058. This figure suggests that the kinetic energy in the Galactic North Galactic Pole emission is more evenly distributed in velocity than that in NGC 1058.